3-D Printed Perforated Conformal Broadband Frequency Selective Surface-Based Absorber

Guna Sai Kiran Nekkanti[1], Gaurav Chaitanya[1,2], Paritosh Peshwe[1], and Saptarshi Ghosh[3]

[1]Department of Electronics and Communication Engineering, Indian Institute of Information Technology, Nagpur, India
[2]Department of Electronics and Communications Engineering, Acropolis Institute of Technology and Research, Indore, India
[3]Department of Electrical Engineering, Indian Institute of Technology, Indore, India

Corresponding Author: Guna Sai Kiran Nekkanti, gunasaikiran8055@gmail.com, 9676345236

Notes on contributors:

Guna Sai Kiran Nekkanti earned his Bachelor's degree in Electronics & Communication Engineering in 2024 from IIIT Nagpur. He is currently pursuing a Master's degree in Electronics & Communication Engineering at IISc Bangalore. His research interests focus on Frequency Selective Surfaces (FSS) and Absorber design.

Gaurav Chaitanya earned his Bachelor's degree in Electronics & Communication Engineering in 2007, followed by a Master's degree from IES, IPS Academy, Indore (affiliated with RGPV, Bhopal, India) in 2012. He has over 16 years of teaching experience at the Acropolis Institute of Technology and Research, Indore, India. He completed his Ph.D. in 2024 from the Indian Institute of Information Technology, Nagpur, India. He holds Senior Membership at IEEE and Life Membership at ISTE. His research interests encompass Frequency Selective Surfaces (FSS), Metamaterials, and Absorber design.

Dr. Paritosh Peshwe completed his MTech in Microelectronics from BITS, Pilani in 2013, and attained his PhD in Antenna Design from VNIT, Nagpur in 2019. His expertise lies in Antenna Design and Wireless Communication. Currently, he serves as an Assistant Professor in the Department of Electronics and Communication Engineering at the Indian Institute of Information Technology, Nagpur, and is a member of IEEE.

Dr. Saptarshi Ghosh holds an MTech and PhD in Electrical Engineering from the Indian Institute of Technology, Kanpur, India, awarded in 2013 and 2017 respectively. He subsequently worked as a Postdoctoral Research Fellow at Chung-Ang University, Seoul, Korea, before joining the Indian Institute of Technology Indore, Madhya Pradesh, India, where he presently serves as an Assistant Professor. His

research expertise spans electromagnetics, frequency selective surfaces, reconfigurable circuits, and metasurfaces. Dr. Ghosh actively contributes as a referee for various IEEE Journals and Conferences, and he holds membership in IEEE and serves as an Associate Editor of IEEE Antennas and Wireless Propagation Letters.

3-D Printed Perforated Conformal Broadband Frequency Selective Surface-Based Absorber

Abstract: This article presents a novel design for a 3-D printed conformal absorber based on frequency selective surface (FSS) concept, which exhibits excellent broadband performance and flexibility. The absorber incorporates an innovative design element printed on a PLA dielectric, supported by a perforated substrate and an air gap, that makes it lightweight while maintaining high absorptivity. Resistive ink is used to print the design pattern on the PLA substrate and a comprehensive parametric analysis is carried out through simulation to meticulously evaluate each design parameter's impact. The geometry demonstrates a remarkable absorption bandwidth covering frequencies from 8.5 GHz to 29.2 GHz (having a fractional bandwidth of 109.81%), with absorption levels consistently exceeding 90%. The design offers broad coverage, spanning the X, Ku, and K bands, and exhibits polarization insensitivity, ensuring effectiveness across various incident wave polarizations. Additionally, the absorber remains stable under oblique incidence for both transverse electric (TE) and transverse magnetic (TM) modes up to 45 degrees of incident angle, making it ideal for a range of practical applications that require conformal and flexible electromagnetic absorption. An equivalent circuit model is created as well as surface current distributions are studied to understand the mechanism of the proposed absorber in detail. Finally, the absorber has been fabricated using a low-cost 3-D printing technology and the measured results has been demonstrated that aligns well with the simulated ones.

Keywords: 3-D printing, perforated geometry, broad-band absorber, flexible absorber

Introduction

Electromagnetic (EM) wave absorbers are widely used in many different sectors, including anechoic chambers, stealth technology, reducing radar cross section (RCS), EM wave compatibility, and EM wave interference (Bahret, 1993; Beeharry et al., 2018). The microwave absorption of earlier conventional absorbers, such as ferrite tile, carbon nanotube, Salisbury screen (Fante, and McCormack, 1988), and Jaumann absorber (Knott, and Lunden, 1995), came at the cost of being thick and heavy. These absorbers are essentially basic radar absorbers,

consisting of a resistive sheet spaced away from the metal surface. Since they only match at one frequency, they have a relatively narrow absorption bandwidth while having a simple structure (Park, Choi, and Kim, 2000; Naito, and Suetake, 1971). With the advent of frequency selective surface (FSS), different types of absorber geometries have been developed, owing to their simple design, low cost, and easy fabrication method.

Earlier FSS absorbers are mostly narrow-band in nature due to their resonance mechanisms. New technologies have made it possible to create circuit analog (CA) absorbers with broad absorption bands by printing periodic resistive-conductive patterns on dielectric surfaces (Yang, and Liang, 2011; Lim, Lee, and Lim, 2016; Wang et al., 2015). Because of it substantial ohmic loss, the resistive elements absorb incident electromagnetic waves over a wide frequency range, while the grounded dielectric substrates aid in impedance matching.

These high-impedance surfaces are widely used to create broadband absorbers due to their greater efficiency (Costa, Monorchio, and Manara, 2007; Costa, Monorchio, and Manara, 2010; Zhang et al., 2013). The capacitive circuit (CC) method is another alternative broadband absorber design technique that has been introduced using multi-layer technology (Kazemzadeh, and Karlsson, 2009). These CA and CC absorbers can be implemented in several ways, such as by painting resistive inks (Chaitanya, and Chandachoriya, 2020) or attaching lumped resistors (Yoo, and Lim, 2014) or with resistive coatings (Zhang et al., 2017). Nevertheless, the initial pair of methods are comparatively costly, delicate when it comes to fabricating massive arrays and challenging to utilize in outdoor settings. Conversely, resistive ink can achieve broadband absorption by being uniformly printed (on any of the dielectric substrates) using a number of affordable technologies (Ghosh, and Lim, 2018). The majority of CA-based broadband absorbers have been built using printed circuit board (PCB) etching techniques on dielectric substrates that are readily available in the market. Not only the total weight of the dielectric may be reduced by careful management during the printing process (Huang et al., 2017), but by selecting appropriate substrate patterns, the structure can also be made mechanically stable.

Additionally, the 3-D printing process is more economical in terms of production time, chemical waste, and fabrication costs when compared to PCB etching. (Ahmadloo, and Mousavi, 2013; Yoon et al., 2018) A few 3-D printed microwave absorber structures have recently been realized using stand-up resistive film arrays, in which the substrate sidewalls are coated with resistive patches (Choi et al., 2014; Jiang et al., 2018). However, those geometries suffer from

large thickness despite having a wide absorption band because several standing wave modes cause the absorptions. Furthermore, the majority of these constructions lack strong mechanical components that make them unsuitable for use in real-world situations. (Shen et al., 2015) Designers have recently focused on using perforated dielectrics based on honeycomb structures and other materials to provide mechanical stability as well as lightweight characteristics to their designs (Ghosh, and Lim, 2018; Liu, and Lan, 2017). Nevertheless, the substrates used to create these kinds of broadband absorbers are stiff and do not conform to curved surfaces. This constraint limits the practical applicability of metamaterial absorbers to some degree. Consequently, researchers have created conformal and flexible FSS-based absorbers, but the primary limitation with those absorbers is their narrow bandwidths (Lai et al., 2018; Jang et al., 2014; Kong et al., 2017; Yahiaoui et al., 2013). A few geometries have employed different materials, such as rubber to achieve a wide bandwidth (wang et al., 2017; Kalraiya et al., 2019), but no study has been done on conformal broadband absorbers utilizing resistors or resistive inks and 3-D printing technology.

This work presents the development of a lightweight FSS-based absorber using 3-D printing technology. A conformal, broadband, ultra-thin, polarization- insensitive microwave absorber is presented in this work. To achieve broadband absorption, a lossy resistive ink has been uniformly painted in resonant loop patterns. The suggested design is implemented on a multi-layer topology, consisting of a solid PLA, perforated PLA, and an air spacer, thereby giving the design mechanical stability as well as structure conformability. The suggested absorber is made to capture above 90% of incident EM waves between 8.74 and 29.07 GHz, which covers the whole X–band (8-12 GHz), Ku–band (12-18 GHz), K-band (18-26 GHz) and partial Ka-band (26-40 GHz). At the lowest operational frequency, the absorber has a total thickness of only 0.015λ, making it very thin. It is still possible to get high absorption when the angle of incidence rises from 0◦ to 45◦ for both TE and TM modes.

Design Analysis:

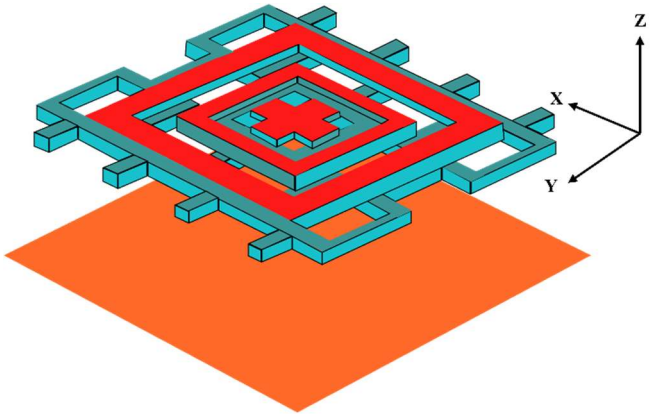

Figure 1: Schematic geometry of the proposed broadband absorber

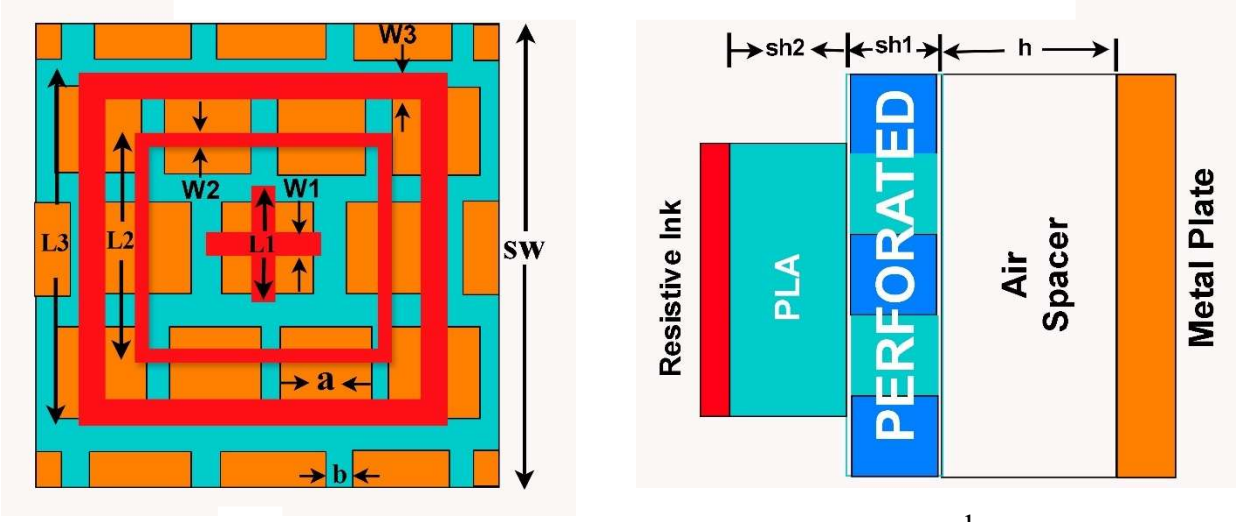

a b

Figure 2: Unit cell geometry of the proposed wideband absorber: (a) top view, and (b) side view.

Figures 1, 2a, and 2b depict the three-dimensional perspective, front, and side view, respectively, of a unit cell of the proposed broadband perforated absorber. This unit cell is periodically extended in lateral directions (x and y-directions), while the EM wave is incident from the top (z-direction). Two perforated layers of PLA substrate (dielectric constant $\varepsilon r = 2.1$ and loss tangent $\tan\delta = 0.07$) with a thickness of sh1 and sh2, are used to build the proposed absorber. The upper layer is used for coating the resistive ink and the lower layer is made perforated for attaining the conformal behavior. In contrast to other 3-D printed structures, the resistive ink is applied in a periodic pattern parallel to the incident wave's transverse direction. The resonating pattern comprises two nested square loops and one plus shape design, effectively dissipating the coupled

electromagnetic energy to heat through ohmic loss. The resistive ink utilized in the structure is Y-shield (σ = 2800 S/m), with an ink layer thickness of 20 microns. Below the PLA layers, an air gap is provided followed by a copper ground plane (metal plate) of thickness mt at the substrate's back side. Table 1 displays the structure's optimal dimensions.

Table 1: Design Parameters in mm.

L1	L2	L3	W1	W2	W3	sh1	sh2	h	sw	a	b	mt
2.2	4.1	7.2	1	0.5	0.8	0.5	1	2	10	2	0.5	0.065

The performance of a broadband absorber depends on the total absorption in the target frequency range. The full-wave simulation of the proposed FSS-based broadband absorber is carried out using Finite Integration Technique (FIT)-based Computer Simulation Technology (CST) software. Boundary conditions are applied along the x, and y directions while maintaining an open boundary along the z-direction to extract the S parameters from the designed absorber.

The S-parameter magnitudes, i.e. the transmission coefficient S21(w) and reflection coefficient S11(w) are examined, and the absorption A(w) is determined using a mathematical relation (1):

$$A(w) = 1 - |S_{11}(w)|^2 - |S_{21}(w)|^2. \quad (1)$$

The reflection coefficient S11(w) and transmission coefficient S21(w) should be kept as low as feasible to achieve the maximal absorption. One way to accomplish the zero transmission is to use a metal plate at the back, which can prevent the EM wave penetrating it. This results in |S21(w)|=0, and subsequently, (1) can be translated as (2):

$$A(w) = 1 - |S_{11}(w)|^2. \quad (2)$$

It is imperative to maintain a low reflection coefficient S11(w) to obtain a larger absorption response A(w), and the same can be achieved by matching the input impedance of the geometry with the free space impedance. Since the free space impedance Zo = 377Ω or 120π, the proposed absorber's input impedance Z(w) must be equal or substantially equal to Zo at the absorption frequency. The following formula (3) can be used to determine the structure's effective impedance:

$$Z_{eff}(w) = \sqrt{\frac{\mu_{eff}}{\epsilon_{eff}}} = \sqrt{\frac{(1+S_{11}(w))^2 - (S_{21}(w))^2}{(1-S_{11}(w))^2 - (S_{21}(w))^2}} \quad (3)$$

Where the effective permittivity and permeability are denoted by ϵeff and μeff, respectively.

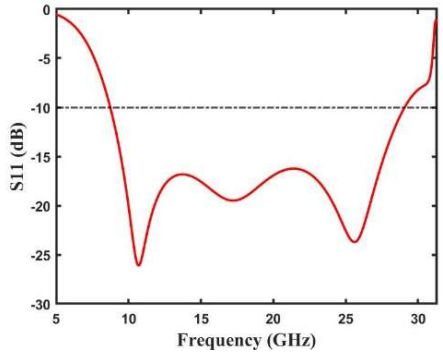

Figure 3: Simulated S 11 (w) of the proposed absorber.

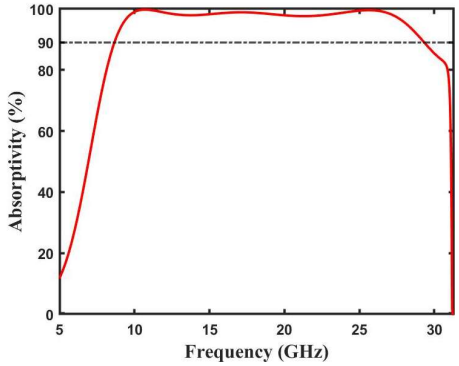

Figure 4: Simulated absorptivity of proposed absorber.

Figure 3 depicts the reflection coefficient S11(w) of the proposed absorber, and its corresponding absorptivity A(w) response is presented in Figure 4. S11(w) is observed below -10 dB over a frequency range from 8.74 to 29.07 GHz, and since S21(w) is equal to zero, a wideband absorption response (above 90% magnitude) is observed for the same frequency range. This results in a fractional bandwidth of 107.54%, which covers the X, Ku, and K bands. The computed S-parameters are further used to calculate the real and imaginary components of the structure's input impedance. Figures 5a and 5b illustrate that the real part of the impedance approaching unity, while the imaginary part nears 0 in the absorption band. Since the absorber's input impedance is almost equal to the impedance of free space (377 + j0) Ω, very less power is reflected from the structure, and maximum power is absorbed at the desired frequency band.

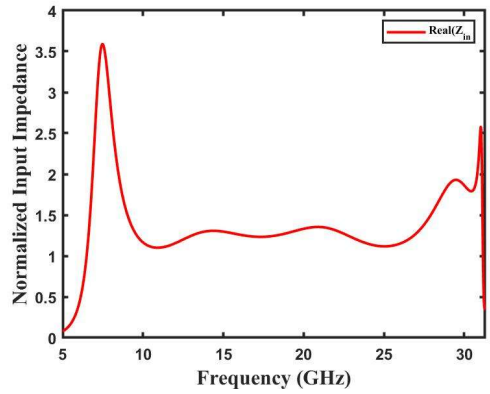

a

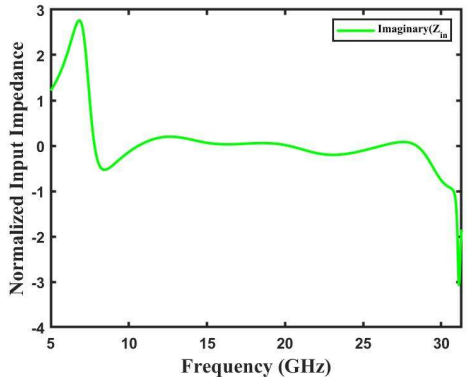

b

Figure 5: Normalized input impedance of the proposed absorber: (a) real part, and (b) imaginary part.

As seen in Figure 6, various modelling scenarios have been investigated to evaluate the effect of absorption response patterns for various regions of the resonating structure. The outer square ring (without the presence of the inner square ring and plus shape) exhibits a smaller amount of bandwidth, covering between 8 to 12 GHz with greater than 90%. The bandwidth gets enhanced in the 8 GHz to 24 GHz range by adding a second square ring inside the outer square element. An additional plus shape inside the inner square ring provides an even wider absorption bandwidth and shows a broadband absorption region of 25 GHz, ranging from 8.74 GHz to 29.07 GHz.

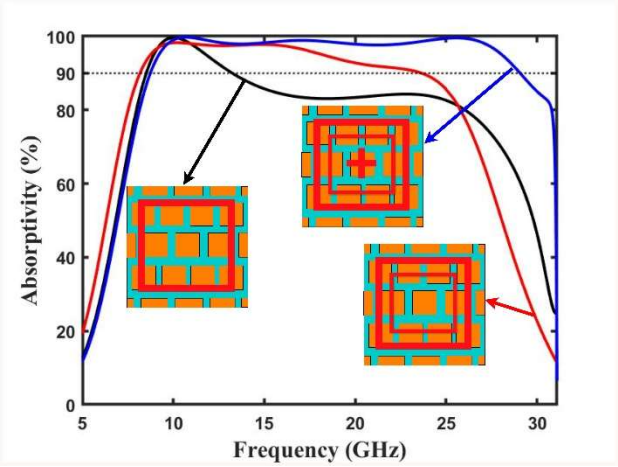

Figure 6: Absorptivity response for different parts of the resonance structure.

Parametric analyses have been carried out on both the resistive ink and the air spacer to better understand their effects on the absorption response, and the results are presented in Figures 7a and 7b, respectively. Figure 7a shows that when the conductivity is increased, the absorption performance first increases but then declines. As a result, the thickness is tuned to 20 μm to attain a high bandwidth. The height of the spacer (h) has been varied from 0 mm to 5 mm with an interval of 1 mm to examine the impact of the free space between the substrate and the ground plane. As the height of the spacer grows, the quarter-wavelength condition gradually shifts to the lower frequency, and as a result, the absorption band also shifts towards the lower frequency side. The spacer height of 2 mm is optimal as it covers the entire X-band, Ku-band, and K-band.

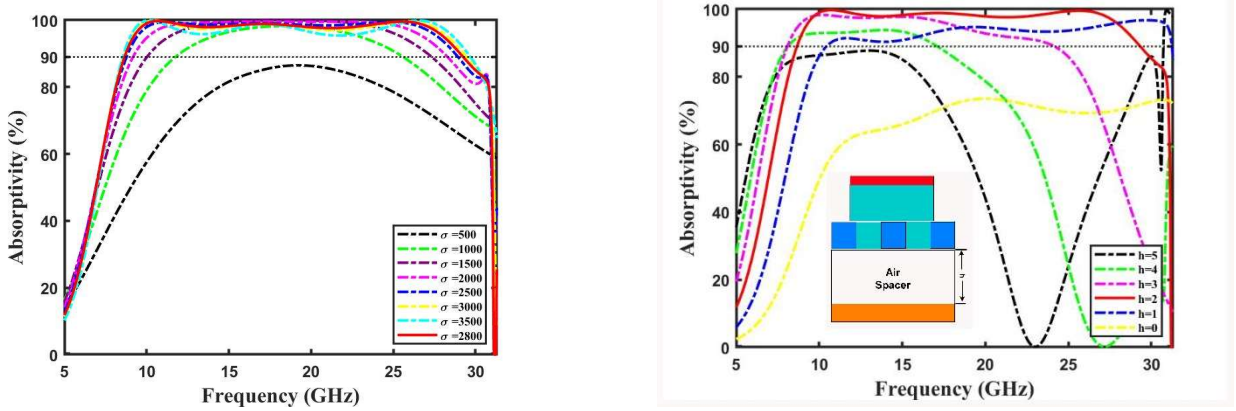

a b

Figure 7: Simulated Absorptivity's for different values of design: (a) Effect of conductivity of the resistive ink (σ), (b) effect of air spacer.

Equivalent Circuit:

An equivalent circuit model has been created to analyze the designed absorber, as shown in Figure 8a. Each of the resonator elements (outer square ring, inner square ring, and plus shape) provides resistance, inductance, and capacitance combined in series. R2-L2-C2, R3-L3-C3, and R1-L1-C1 correspond to the inner and outer loops and inner shape, respectively. The resistances are generated from the lossy characteristics of the resistive ink, while inductances are generated from the top square loop patterns. The gap between the inner loop and the plus shape results in capacitance C1, the gap between the inner and outer loop results in capacitance C2, and the gap between the outer loops across the neighboring unit cells results in capacitance C3. The PLA substrates with thicknesses sh2 and sh1 are modelled as individual transmission line segments, whereas the air spacer is modelled as another transmission line. The ground plane is considered as short circuit. Their corresponding equations are presented in Equations (4)-(11).

$$Z\_\{in\} = ZFSS1 \,||\, ZFSS2 \,||\, ZFSS3 \,||Z_{d1} \tag{4}$$

$$ZFSS1 = R_1 + jwL_1 + \frac{1}{jw_{\ 1}} \tag{5}$$

$$ZFSS2 = R_2 + jwL_2 + \frac{1}{jwC_2} \tag{6}$$

$$ZFSS3 = R_3 + jwL_3 + \frac{1}{jwC_3} \tag{7}$$

$$Z_{d1} = Z_d \frac{Z_{d2} + jZ_d \tan(\beta_d(sh1+sh2))}{Z_d + jZ_{d2} \tan(\beta_d(sh1+sh2))} \quad (8)$$

$$Z_{d2} = jZ_o \tan(\beta h) \quad (9)$$

$$Z_o = \sqrt{\frac{\mu}{\epsilon}} \quad (10)$$

$$Z_d = \frac{Z_o}{\sqrt{\epsilon}} \quad (11)$$

The circuit parameters have also been designed in Advanced Design System (ADS) software and their values are determined using the curve fitting technique, as listed in Table 2. Comparing the reflection coefficient S11(w) obtained from the circuit model with the full-wave simulation, as shown in Figure 8b, reveals good agreement and indicates the accuracy of the circuit model.

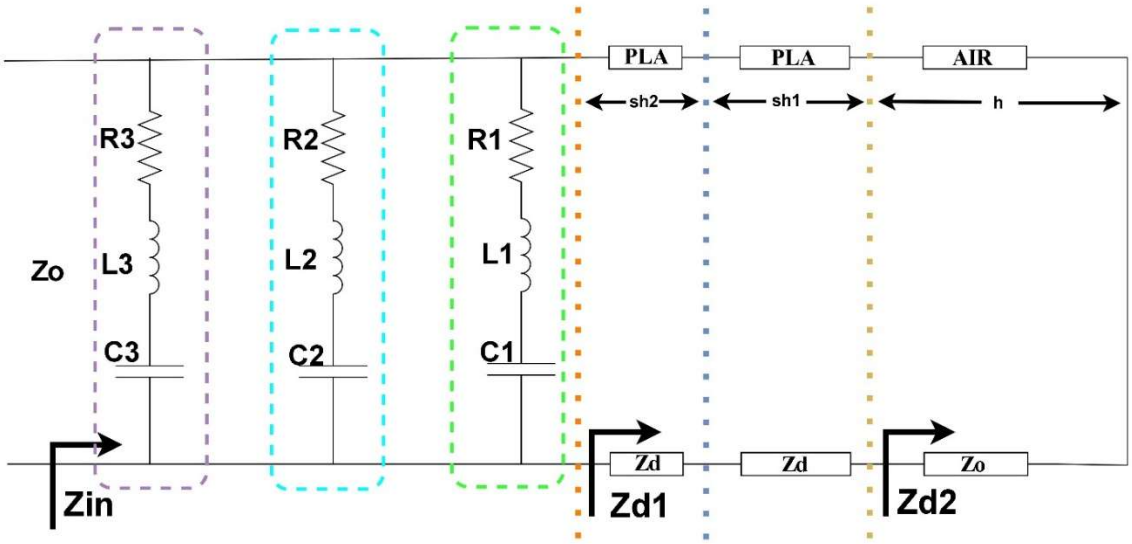

a

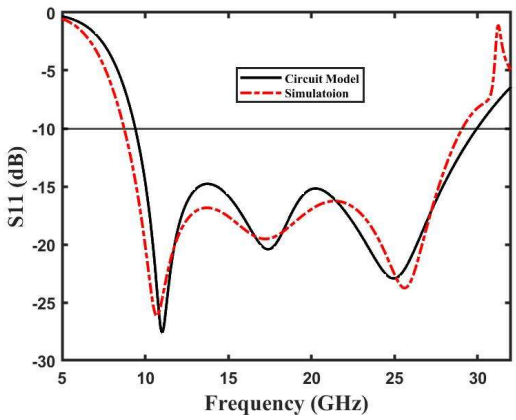

b

Figure 8: (a) Equivalent circuit model, and (b) comparison of simulated and calculated reflection coefficients.

Table 2: Optimized design parameters of Equivalent circuit in Figure 8a

Dimensions (unit: R(Ω), L(nH), C(fF), Z(Ω))		
R1 = 478	L1 = 11.38	C1 = 14.39
R2 = 1085	L2 = 43.8	C2 = 1.5
R3 = 0.065	L3 = 3.4	C3 = 16.9
$Z_o = 377$	$Z_d = \frac{Z_o}{\sqrt{\epsilon_r}} = 260.15$	

Simulated Results:

Study of Polarization-sensitivity:

Absorber structures are generally installed in objects with an aim to reduce the RCS, and the absorption performance should be guaranteed irrespective of the angle of polarization (φ) of the incident EM wave. The proposed geometry has a combination of resistive patterns in the top and perforated layers in the bottom, among which the perforated layer is slightly truncated to ensure the unit cell structure becomes precisely square. However, this minor asymmetry doesn't have any effect in the absorption response, as it remains uniform for all angles of polarization (φ) of the incident EM wave, as shown in Figure 9. Thus, the design can be regarded as polarization-insensitive and is therefore suitable for practical applications.

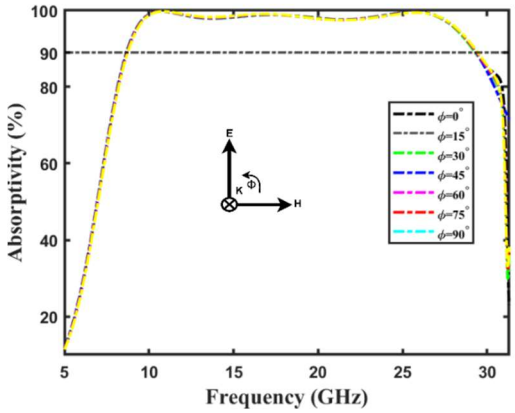

Figure 9: Simulated absorptivity of the proposed broadband absorber for various polarization angles under normal incidence.

Study of oblique incidence behaviour:

The following equations (12) (13) define the reflection coefficients under oblique incidence for TE polarization (Γ⊥) and TM polarization (Γ||).

$$\Gamma_{\perp} = \frac{Z(w)\cos\theta_i - Z_o\cos\theta_t}{Z(w)\cos\theta_i + Z_o\cos\theta_t} \tag{12}$$

$$\Gamma_{\parallel} = \frac{Z(w)\cos\theta_t - Z_o\cos\theta_i}{Z(w)\cos\theta_t + Z_o\cos\theta_i} \tag{13}$$

It can be shown from Equations (12) and (13) that as the incident angle varies, so does the reflection coefficient. Figures 10a and 10b show the absorption responses of the proposed structure for different angles of incidence (θ) under TE and TM polarizations, respectively. As seen in Figure 10a, with the TE polarization, the E-field direction stays constant while the EM wave's propagation direction and the magnetic field's direction rotate at different angles. For TM polarization, the H-field direction stays constant, but the electric field and EM wave propagation directions rotate at different angles. The structure is therefore examined for oblique incidence. Figure 10a illustrates the broadband absorption (absorptivity above 90%) up to a 45◦ angle of incidence for TE mode, while the same is maintained up to 30◦ angle of incidence for TM mode, as shown in Fig 10b. At higher incident angles, the absorption magnitude gradually reduces and the broadband behaviour is moved to a higher frequency.

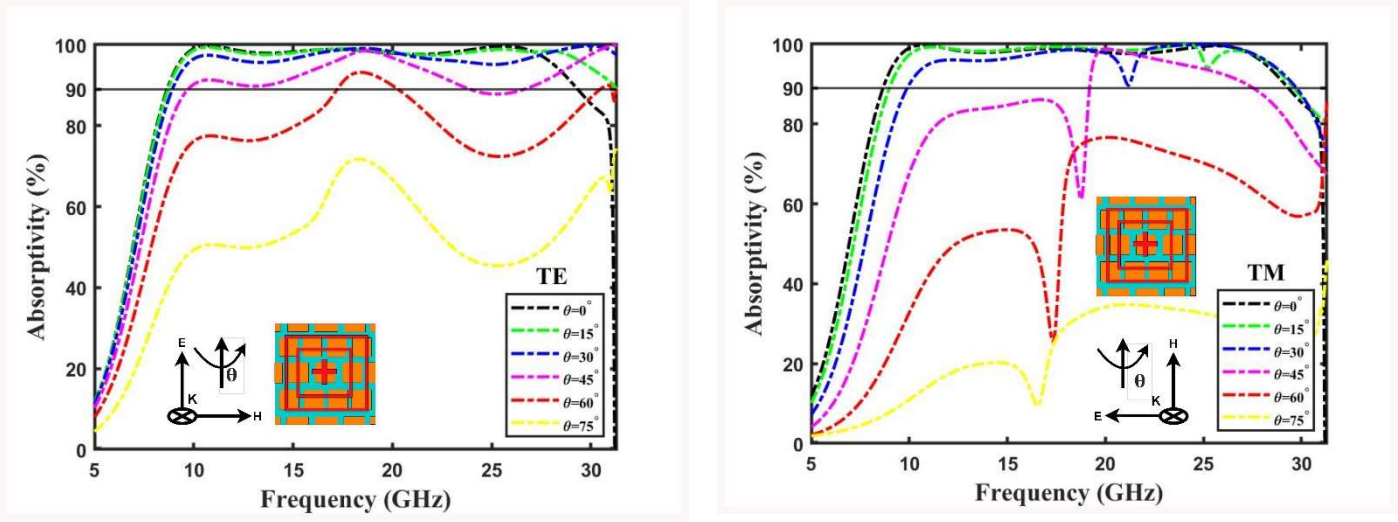

a b

Figure 10: Simulated absorptivity at different incident angles under (a) TE mode, and (b) TM mode.

Current Distribution on unit cell structure:

As seen in Fig 11, the surface currents are investigated at three resonance frequencies: 10.7, 17.4, and 25.7 GHz. Figures 11a and 11b show the surface current for TE and TM modes at 10.7 GHz, respectively. This image shows that magnetic excitation is produced by the antiparallel surface current at the top and bottom side of the suggested unit cell. Comparably, Figures 11c and 11d show the surface current for TE and TM modes at 17.4 GHz, respectively. It is evident that the top and bottom surface currents of the suggested unit cell are parallel, which produces an electric excitation. Figures 11e and 11f show the surface current for TE and TM modes at 25.7 GHz, respectively. Strong EM absorption at these two frequencies will be produced within the structure when the electric and magnetic excitations are combined.

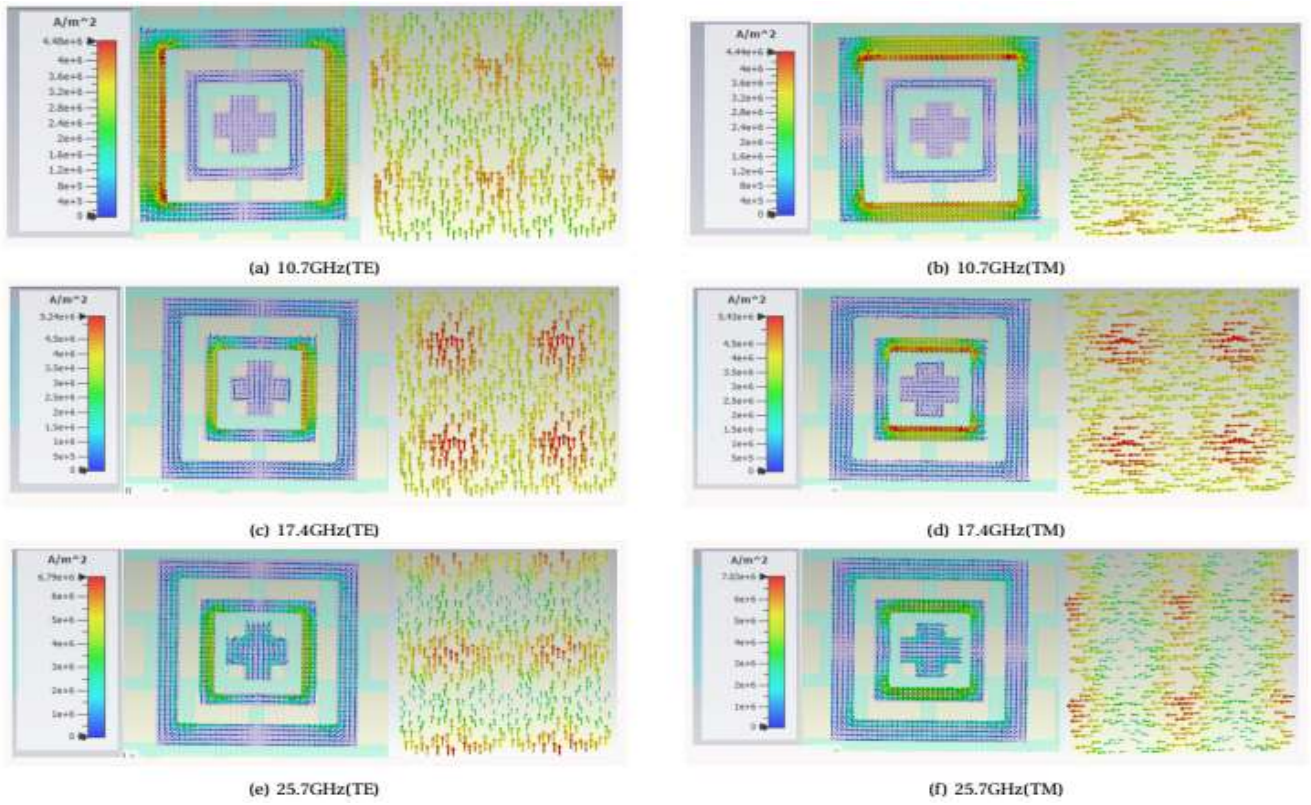

Figure 11: Induced surface current distribution on the top resistive patch and a bottom metallic layer of the unit cell.

Parametric Analysis:

Effect of Perforated Substrate thickness (sh1): In Fig 12a, the absorptivity is demonstrated by varying the perforated PLA substrate layer's thickness (sh1) from 0.7 mm to 0.2 mm, with a 0.1 mm width. It is observed that the absorption bandwidth dramatically drops in the higher frequency range as sh1 increases. Conversely, the conformal behaviour of the structure is lost with larger thickness value. Therefore, a thickness of 0.5 mm has been selected based on the suitability of the substrate layer to attain the highest absorption bandwidth. The substrate is made perforated to realize higher order of flexibility.

Effect of Substrate thickness (sh2): When the top PLA substrate layer thickness (sh2) is changed from 1 mm to 0.1 mm with a 0.2 mm width, the corresponding absorptivity response is depicted in Figure 12b. It is seen that the absorption bandwidth dramatically drops as sh2 increases. However, there is no movement towards higher frequencies. In a similar way, a thickness of 1 mm has been selected to obtain the highest absorption bandwidth while maintaining lesser thickness and greater flexibility.

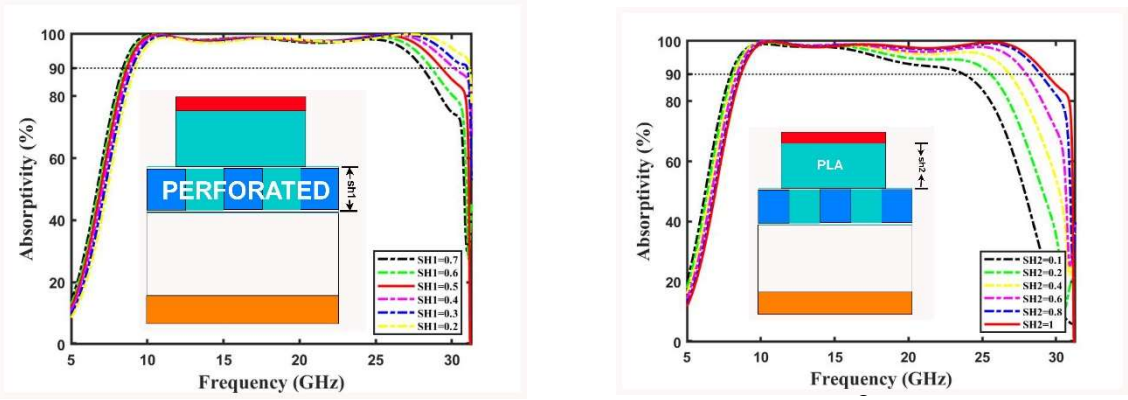

a b

Figure 12: Variation of the different design parameters of the proposed broadband absorber: (a)effect of perforated substrate thickness, and (b)effect of substrate thickness.

Conformal Analysis:

The curvature of an FSS design significantly influences how effectively it can absorb EM wave arriving at various angles. To study the curvature effect, the proposed design has been simulated at three different curvature angles ψ = 90◦, ψ = 135◦, and ψ = 180◦. A 6×6-unit cell configuration has been considered, and wrapped on a cylindrical surface, whose radius of curvature has been varied to attain the above-mentioned curvature angles. The EM wave is incident at Normal incidence for all cases. The simulation setup is illustrated in Figure 13. The corresponding reflection coefficients for different curvature angles are presented in Figure 14. These findings underscore excellent absorption characteristics of the geometry across different curved surfaces, thereby confirming the suitability of the proposed absorber design for curved configurations.

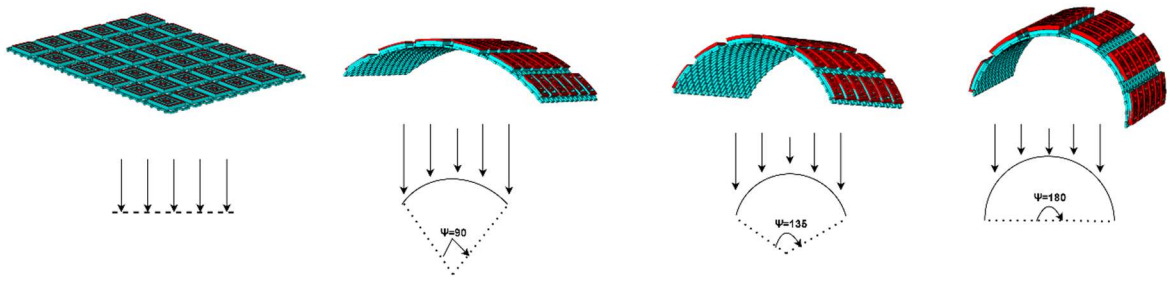

Figure 13: Conformal measurement at different central angles (Ψ).

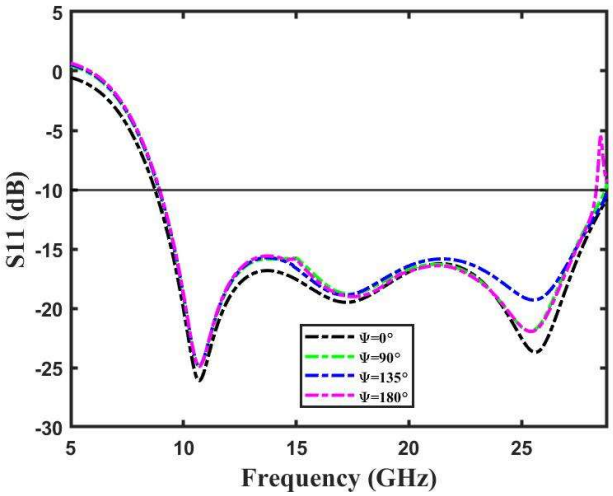

Figure 14: Simulated reflection coefficient curves under different central angles. (Ψ).

Fabrication and Measurement:

A prototype of the proposed broadband absorber was fabricated to verify it experimentally. PLA material was used to create the perforated-shaped dielectric substrate using 3-D printing technology. The substrate was printed using a commercial 3-D printer Ultimaker 2+ from Geldermalsen. After constructing the dielectric layers, Y-shield-resistant ink was applied by hand with a paintbrush. The necessary thickness (around 20 microns) was achieved with just one layer of ink painted on the substrate. To realize the requisite airgap, another thin PLA layer was made and a copper tape of 2 mm thick was pasted covering the entire layer, and a frame was made to hold the copper layer as well as PLA layers together while maintaining the airgap. The fabrication process is illustrated in Figure 15(a), and the photographs of the prototype are presented in Figures 15(b) and 15(c), presenting a 190 × 190 mm sample made up of 19 x 19 unit cells, each measuring 10 mm.

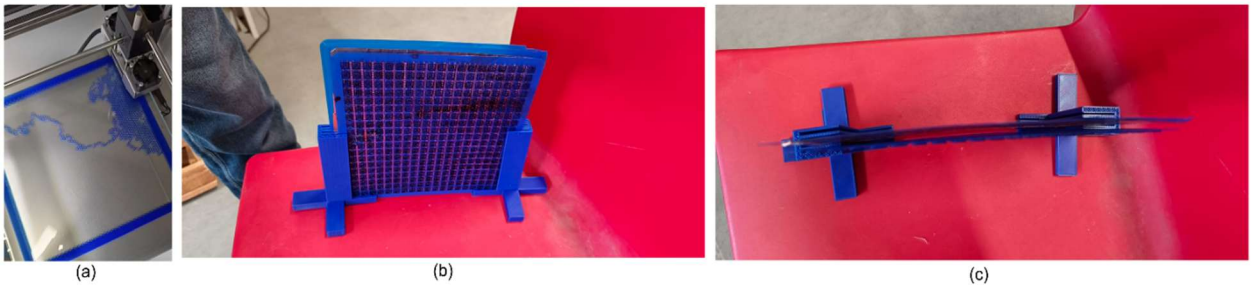

Figure 15: (a) 3-D printing fabrication process. Photograph of the fabricated prototype:

(b) side view, (c) top view.

An anechoic chamber was used to measure the absorptivity response of the fabricated structure. A vector network analyzer (VNA) and two pairs of linearly polarized standard gain broadband horn antennas were used during the experiment. The antennas, one serving as a transmitter and another as a receiver, were placed in proximity facing towards the sample, and the distance between them was maintained at the far-field criterion. Two pairs of antennas were used, one set having a frequency range from 2 to 18 GHz, and the other set having a frequency range from 18 to 0GHz, and the setup is depicted in Figure 16. The estimation of the far-field region is given by far-field >> 2D2, where D is the antenna's largest dimension and λ is the wavelength of the maximum operating frequency. As a result, the antennas and the test sample were placed 1800 mm apart.

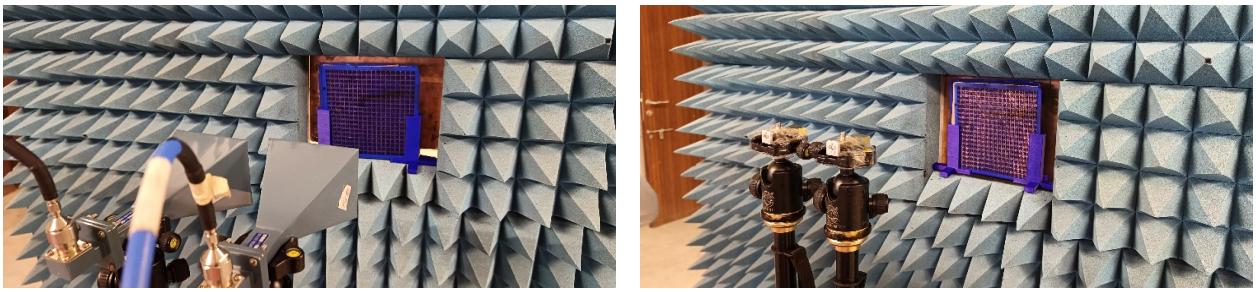

(a) (b)

Figure 16: Measurement setups using different pairs of horn antennas: (a) Horn antenna pair 1 (2-18 GHz), and (b) Horn antenna pair 2 (18-40 GHz).

The calibration was performed using a copper metal plate having the same size as that of the meta surface. Once the setup was made ready, the reflection coefficient from the sample was first measured and then replaced with that of the copper plate. The difference between the reflected powers from the copper sheet (used for calibration) and the fabricated sample was utilized to compute the actual reflection from the structure and the corresponding absorptivity was calculated. The measured and simulated absorptivity under normal incidence is displayed in Figure 17. The overall reflection characteristic of the fabricated prototype matches well with the full-wave simulated response. A small amount of variation is observed, which can be attributed to the manufacturing tolerance, limited sample size, and the dispersive nature of the constituent materials (PLA and Y-shield resistive ink).

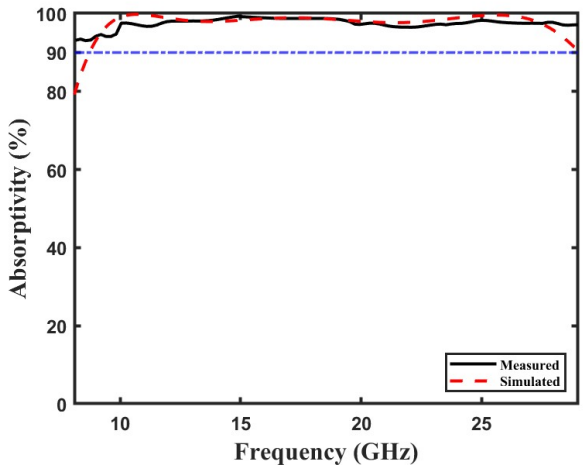

Figure 17: Measured and Simulated absorptivity of the proposed broadband absorber under normal incidence.

Once the structure was measured for planar configuration, with varying central angle (ψ) to experimentally evaluate its conformal performance, as illustrated in Figure 18(a). A flexible foam (ϵr ≈ 1) was used as an air spacer while measuring the reflection coefficient of the sample under different central angles. Figure 18(b) exhibits the corresponding absorption responses across different central angles. A similar full-wave simulation environment has been generated in the software, and corresponding reflection coefficients are determined in the prototype was bent around a cylindrical curved surface Figure 18.

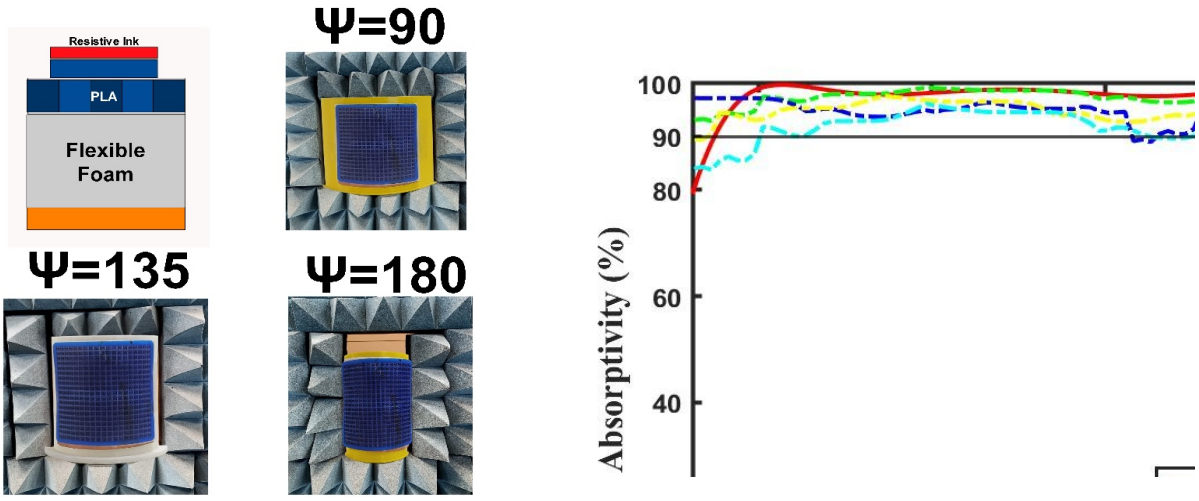

a b

Figure 18: (a) Photograph of bending the absorber sample at different centre angles on a cylindrical surface, and (b) corresponding measured absorptivities at different central angles.

The absorptivity results under the planar as well as conformal configuration indicate the effective performance of the proposed design in the desired frequency range. Therefore, the proposed broadband conformal absorber is highly suitable for use on curved surfaces. Table 3 illustrates how the proposed absorber outperforms the existing designs in terms of bandwidth, flexibility, and cost-effectiveness while comparing it with the previous works. The geometry achieves superior compactness and broader bandwidth as compared to previously reported broadband absorber structures, without relying on lumped elements. Moreover, the design introduces a novel conformal nature that previous researchers had not explored. This combination of

attributes underscores the advancements made by our proposed absorber, marking a significant leap forward in the absorber technology due to its innovative design and novel conformal nature.

Table 3: Comparison Table

References	**Unit cell size (mm)**	**Dielectric thickness (mm)**	**Centre Freq (GHz)**	**Air Space (mm)**	**Use of Resistor**	**-10 dB Band-width (GHz)**	**Conformal**	**Angular Stability (>90)**
(Ghosh, and Lim 2018)	16	5.5	11.24	0	NO	11.44	NO	45 for TE
(Chaitanya, and Chandachoriya 2020)	10	0.3	9.1	7	YES	5.7	NO	30 for TE
(Ghosh, Bhattacharyya, and Srivastava 2016)	13	1.6	11.59	3	YES	13.5	NO	30 for TE
(Kong et al. 2017)	14.4	0.18	9.56	3.5	YES	7.04	YES	30 for TE
(wang et al. 2017)	15.8	0.125	12.93	2.5	NO	12.14	YES	NA
(Kalraiya et al. 2019)	12.5	0.07	7.2	7.5	YES	6.6	YES	45 for TE
(Malik, Sharma, and Srivastava 2021)	10	1.58	5.78	16.36	NO	5.25	NO	30 for TE
(Tiwari, Pathak, and Anitha 2021)	10.6	0.2	13	5	NO	10	YES	50 for TE
(Yang et al.	12	2.6	10	0	NO	4.8	YES	45 for TE

2023)								
(Kumari et al. 2024)	16	0.3	14.2	4	NO	15.82	NO	45 for TE
This Work	10	1.5	18.9	2	NO	20.34	YES	45 for TE

Conclusion

A conformal broadband polarization-independent and angularly stable FSS-based absorber has been presented. The design uses 3-D printing technique to create perforated dielectric layers, which is coated with a lossy resistive ink to achieve broadband absorption response. When contrasted with its equivalent (i.e. a similar topology but made of solid PLA material), the proposed design is lightweight, low cost, as well as, exhibits a wideband absorption behaviour for both flat and curved surfaces in the frequency range of 8.5 GHz to 29.2 GHz (fractional absorption bandwidth = 109.81%). The provided to help comprehend the absorption mechanism. For both TE and TM polarizations, the structure provides a broadband absorption for an oblique incidence angle of up to 45o. The fabricated prototype was tested in real-world conditions on flat and curved surfaces, confirming it absorption behaviour in the desired frequency range, as predicted by simulations. This successful demonstration confirms that the proposed design can be used in various applications in defense, telecommunications, and aerospace industries, like protecting against EM waves, improving stealth for targets, and reducing radar visibility.

Funding

This research received no external funding.

Declaration of Interests

The authors declare that they have no known competing financial interests or personal relationships that could have appeared to influence the work reported in this paper.

Acknowledgments

The authors would like to extend their sincere appreciation to the Electrical Department and the Applied Electromagnetic Laboratory at the Indian Institute of Technology Indore for their invaluable assistance in the fabrication and testing phases of this research project. Their expertise and support were instrumental in the successful completion of this endeavor.

References

W. F. Bahret, IEEE Trans. Aerosp. Electron. Syst. 29, 1377 (1993).

T. Beeharry, R. Yahiaoui, K. Selemani, and H. H. Ouslimani, Materials 11,1668 (2018).

Ghosh, S., Bhattacharyya, S., & Srivastava, K. V. (2016). Design, characterization and fabrication of a broadband polarisation-insensitive multi-layer circuit analogue absorber. IET Microwaves Antennas & Propagation, 10(8), 850–855.

R. L. Fante and M. T. McCormack, IEEE Trans. Antennas Propag. 36, 1443 (1988).

E. F. Knott and C. D. Lunden, IEEE Trans. Antennas Propag. 43, 1339 (1995).

M. J. Park, J. Choi, and S. S. Kim, IEEE Trans. Magn. 36, 3272 (2000).

Y. Naito and K. Suetake, IEEE Trans. Microw. Theory Tech. 19, 65 (1971).

L. Li, Y. Yang, and C. Liang, "A wide-angle polarization-insensitive ultra-thin meta-material absorber with three resonant modes," J. Appl. Phys., vol. 110, no. 6, p. 063702, Sept. 2011.

D. Lim, D. Lee, and S. Lim, "Angle- and polarization-insensitive metamaterial absorber using via array," Sci. Rep., vol. 6, p. 39686, Dec. 2016

B. Wang, B. Y. Gong, M. Wang, B .Weng, and X. Zhao, "Dendritic wideband metamaterial absorber based on resistance film," Appl. Phys. A, vol. 118, no. 4, pp. 1559-1563, Mar. 2015.

F. Costa, A. Monorchio, and G. Manara, "Ultra-thin absorber by using high impedance surfaces with frequency selective surfaces," Proc. IEEE Int. Symp. on Antennas Propag., Honolulu, 2007, pp. 861–864.

F. Costa, A. Monorchio, and G. Manara, "Analysis and design of ultrathin electromagnetic absorbers comprising resistively loaded high impedance surface," IEEE Trans. Antennas Propag., vol. 58, no. 5, pp. 1551–1558, May 2010.

H. B. Zhang et al., "Resistance selection of high impedance surface absorbers for perfect and broadband absorption," IEEE Trans. Antennas Propag., vol. 61, no. 2, pp. 976-979, Feb. 2013.

A. Kazemzadeh and A. Karlsson, "Capacitive circuit method for fast and efficient design of wideband radar absorbers," IEEE Trans. Antennas Propag., vol. 57, no. 8, pp. 2307–2314, Aug. 2009.

M. Yoo and S. Lim, “Polarization-independent and ultrawideband metamaterial absorber using a hexagonal artificial impedance sur- face and a resistor-capacitor layer,” IEEE Trans. Antennas Propag., vol. 62, no. 5, pp. 2652-2658, Feb. 2014.

C. Zhang, Q. Cheng, J. Yang, J. Zhao, and T. J. Cui, “Broadband metamaterial for optical transparency and microwave absorption,” Appl. Phy. Lett., vol. 110, p. 143511, Apr. 2017

G. Chaitanya and A. Chandachoriya, "Polarization Independent Super Thin Metamaterial Microwave Broadband Absorber for X-Band Application," 2020 IEEE 9th International Conference on Communication Systems and Network Technologies (CSNT), Gwalior, India, 2020, pp. 13-18, doi: 10.1109/CSNT48778.2020.9115751.

Ghosh, Saptarshi, and Sungjoon Lim. "Perforated lightweight broad-band metamaterial absorber based on 3-D printed honeycomb." IEEE Antennas and Wireless Propagation Letters 17, no. 12 (2018): 2379-2383.

G. L. Huang, S. G. Zhou, C. Y. D. Sim, T. H. Chio, and T. Yuan, “Lightweight perforated waveguide structure realized by 3-D print- ing for RF applications,” IEEE Trans. Antennas Propag., vol. 65, no. 8, pp. 3897- 3904, Aug. 2017

M. Ahmadloo and P. Mousavi, “A novel integrated dielectric- and conductive ink 3D printing technique for fabrication of mi- crowave devices,” IEEE MTT-S International Microwave Symposium Digest, pp. 1-3, 2013.

Y. Yoon, D. Lim, M. M. Tentzeris, and S. Lim, “Low-cost metama- terial absorber using three-dimensional circular truncated cone,” Microw. Opt. Technol. Lett., vol. 60, pp. 1622-1630, May 2018.

W.-H. Choi, J.-H. Shin, T.-H. Song, W.-Y. Lee, W.-J. Lee, and C.-G. Kim, “Design of broadband microwave absorber using honeycomb structure,” Electron. Lett., vol. 50, no. 4, pp. 292-293, Feb. 2014.

W. Jiang et al., “Electromagnetic wave absorption and compressive behavior of a three-dimensional metamaterial absorber based on 3D printed honeycomb,” Sci. Rep., vol. 8, p. 4817, Mar. 2018.

Y. Shen et al., “Origami-inspired metamaterial absorbers for improv- ing the larger-incident angle absorption,” J. Phys. D Appl. Phys., vol. 48, p. 445008, Oct. 2015.

P. Liu and T. Lan, Appl. Opt. 56, 4201 (2017).

T. Jang, H. Youn, Y. J. Shin, and L. J. Guo, ACS Photonics 1, 279 (2014)

S. Lai, Y. Wu, J. Wang, W. Wu, and W. Gu, Opt. Mater. Express 8, 1585 (2018).

X. Kong, J. Xu, J. J. Mo, and S. Liu, Front. Optoelectron. 10, 124 (2017).

R. Yahiaoui, J. P. Guillet, F. D. Miollis, and P. Mounaix, Opt. Lett. 38, 4988 (2013).

Wang, Ling-ling & Liu, Shao-Bin & Feng, Zhang & Kong, Xiang-Kun & Liu, Lu-lu. (2017). High-impedance surface-based flexible broadband absorber. Journal of Electromagnetic Waves and Applications. 31. 1-16. 10.1080/09205071.2017.1326850.

Kalraiya, S., Chaudhary, R.K. and Abdalla, M.A., 2019. Design and analysis of polarization independent conformal wideband meta- material absorber using resistor loaded sector shaped resonators. Journal of Applied Physics, 125(13).

Malik, S., Sharma, A., & Srivastava, K. V. (2021). Resistive Ink Based Microwave Absorber for S and C-Band with 99% Absorption. 2021 IEEE Indian Conference on Antennas and Propagation (InCAP) https://doi.org/10.1109/incap52216.2021.9726447

Tiwari, P., Pathak, S. K., & Anitha, V. P. (2021). Design, development and characterization of wide incidence angle and polarization insensitive metasurface absorber based on resistive-ink for X and Ku band RCS reduction. Waves in Random and Complex Media, 34(4), 3161–3176. https://doi.org/10.1080/17455030.2021.1972182

Yang, Yalan & Song, Chaoyun & Pei, Rui & Wang, Jianping & Liu, Zhe & Zhang, Youran & Shen, Jinzhu. (2023). Design, Characterization and Fabrication of a Flexible Broadband Metamaterial Absorber Based on Textile. 10.1016/j.addma.2023.103537.

Kumari, N. B., Kumar, N. A., Kumar, N. P., & Singh, N. M. (2024). Polarization Independent Ultra-wideband Meta-material Absorber Using Conductive Ink Resonator. Journal of Telecommunications and Information Technology, 1, 39–45. https://doi.org/10.26636/jtit.2024.1.1392